Molecular Biology of the Cell
Vol. 21, 4264–4274, December 1, 2010

C-jun Inhibits Mammary Apoptosis In Vivo

Sanjay Katiyar,*† Mathew C. Casimiro,* Luis Dettin,‡ Xiaoming Ju,* Erwin F. Wagner,§ Hirokazu Tanaka,‖ and Richard G. Pestell*†

Departments of *Cancer Biology and †Medical Oncology, Thomas Jefferson University, Philadelphia, PA 19107; ‡Department of Neuroscience, Georgetown University, Washington, D.C. 20057; §BBVA Foundation, CNIO Cancer Cell Biology Programme, E-28029 Madrid, Spain; and ‖Department of Regenerative Medicine, Institute of Biomedical Research and Innovation, Kobe, 650-0047, Japan

Submitted August 16, 2010; Revised September 23, 2010; Accepted September 28, 2010
Monitoring Editor: Kunxin Luo

***c-jun*, which is overexpressed in a number of human cancers encodes a critical component of the AP-1 complex. *c-jun* has been shown to either induce or inhibit cellular apoptosis. Germ line deletion of both *c-jun* alleles is embryonically lethal. To determine the role of the endogenous *c-jun* gene in apoptosis, we performed mammary epithelial cell–targeted somatic deletion using floxed *c-jun* (*c-jun*$^{f/f}$) conditional knockout mice. Laser capture microdissection demonstrated endogenous *c-jun* inhibits expression of apoptosis inducing genes and reactive oxygen species (ROS)-reducing genes (MnSOD, catalase). ROS have been implicated in apoptosis and undergo enzymatic elimination via MnSOD and CuZnSOD with further detoxification via catalase. *c-jun*–mediated survival was in part dependent on ROS production. *c-jun*–mediated repression of MnSOD and catalase occurred via mitochondrial complex I and NOX I. Collectively, these studies define a pivotal role of endogenous *c-jun* in promoting cell survival via maintaining mitochondrial integrity and expression of the key regulators of ROS production.**

INTRODUCTION

The *c-jun* oncoprotein is an essential component of an activator protein transcription complex. On hetero-dimerization with other Jun/Fos members it forms an active activator protein -1 complex (AP-1), which regulates the expression of various target genes harboring AP-1–binding DNA elements within their promoters. AP-1 controls the expression of genes that regulate several crucial cellular functions such as cell cycle progression, migration, proliferation, and apoptosis. *c-jun* is activated upon phosphorylation by *c-jun* N-terminal kinase (JNK), which responds to diverse biological stress signals (Kyriakis, 1999).

c-jun functions as both a positive and negative regulator of apoptosis (Shaulian and Karin, 2002). Nerve growth factor (NGF) withdrawal induced neuronal apoptosis is reduced by *c-jun* inhibition, and mice expressing the *c-jun* phosphorylation site mutant (*c-jun* A63/73) are resistant to kainate seizure-induced apoptosis (Ham *et al.*, 1995; Behrens *et al.*, 1999). In contrast, *c-jun* inhibits TNF-α–induced apoptosis via p53/p21 in transformed fibroblasts (Eferl *et al.*, 2003), and p53 is induced in *c-jun*$^{-/-}$ liver tumors. p53 however is not activated in *c-jun*$^{-/-}$ hepatocytes (Eferl *et al.*, 2003), suggesting acute *c-jun* deficiency induces apoptosis eliminating p53-overexpressing cells.

Reactive oxygen species (ROS) are thought to play an important role in cell death: apoptosis, programmed necrosis, cellular proliferation, premature senescence, genomic instability, and cellular invasiveness. On one hand, ROS induced by oncogenic Ras or ErbB2 has been shown to induce antiproliferative signals that block cellular proliferation and growth (Dolado *et al.*, 2007). ROS can cooperate with oncogenic signals and in some circumstances ROS production is associated with activation of growth receptors including transforming growth factor-β and platelet-derived growth factor (PDGF; Sattler *et al.*, 1999; Balaban *et al.*, 2005). The carcinogenic effect of ROS has been linked to increased cellular proliferation rate seen in many cancer cell lines (Fernandez-Pol *et al.*, 1982; Church *et al.*, 1992). Mitochondria are the major source of cellular ROS, derived from leakage of electrons from carriers in the electron transport chain (Scherz-Shouval *et al.*, 2007) produced during the turnover of complex I and complex II. Molecular oxygen is converted to superoxide (O_2^-), which in turn develops into ROS. Non-mitochondrial ROS are derived from other compartments including peroxisomes, plasma membrane, the endoplasmic reticulum, Golgi complex, lysosomes, and the nucleus. ROS may be generated by reduced nicotinamide adenine dinucleotide phosphate (NADPH) oxidases, which includes a catalytic subunit of the NADPH oxidase (NOX) family (Lambeth, 2004). ROS formation and efflux may be altered by the mitochondrial inner transmembrane potential (Δ^{ψ_m}), pH gradient and the outer mitochondrial membrane potential, O_2^- production is enhanced by high Δ^{ψ_m} ROS leave the mitochondria either via diffusion or via active carriers such as the inner membrane anion channel (IMAC) or the voltage-dependent anion channel (VDAC; Boveris and Chance, 1973).

This article was published online ahead of print in *MBoC in Press* (http://www.molbiolcell.org/cgi/doi/10.1091/mbc.E10–08–0705) on October 6, 2010.

Address correspondence to: Richard G. Pestell (richard.pestell@jefferson.edu).

Superoxide dismutases are the antioxidant enzymes that catalyze the dismutation of O_2 to H_2O_2. There are two forms of intracellular superoxide dismutases (SODs) in mammalian cells: nuclear and cytoplasmic CuZnSOD (SOD-1) and mitochondrial matrix localized MnSOD (SOD-2).

In addition to passive or active diffusion from mitochondria, ROS undergo enzymatic elimination via MnSOD (Melov, 2000) or CuZnSOD (Okado-Matsumoto and Fridovich, 2001). Further detoxification is undertaken by glutathione peroxidase (GPX; Nohl and Jordan, 1980) which uses reduced glutathione (GSH) and/or catalase in which converts H_2O_2 to H_2O (Radi *et al.*, 1991).

The *c-jun* gene plays a central role in the diverse functions of the AP-1 complex. Although the number of studies is small, analysis of acute loss of target genes have revealed distinct results compared with germ line deletion studies (Sage *et al.*, 2003). The current studies were conducted first, therefore, to determine the signaling pathways regulated by endogenous *c-jun* in vivo. To this end, *c-jun*$^{fl/fl}$ mice were deployed, and excision was conducted using cre recombinase. Laser capture microdissection (LCM) was conducted of cells deleted of *c-jun*, and genome-wide expression analysis was conducted to determine signaling pathways regulated by *c-jun* in vivo. Second, *JNK* and the *c-jun* genes have been linked to both the inhibition and induction of cellular apoptosis (Xia *et al.*, 1995; Kuan *et al.*, 1999; Xia and Karin, 2004). The current studies were therefore conducted to examine the effect of acute *c-jun* excision on cellular survival.

MATERIALS AND METHODS

Transgenic Mice and Expression Plasmids

Transgenic animals carrying floxed c-*jun* alleles, c-*jun*$^{f/f}$, and mouse mammary tumor virus (MMTV)-Cre were previously described (Zenz *et al.*, 2003). The mammary gland mRNA was obtained from virgin female mice at 2 mo of age. All experimental procedures conducted on these mice were approved by the ethics committee of Thomas Jefferson University. Quantitation of mammary epithelial cell number was conducted as described (Atabai *et al.*, 2005). Apoptosis in situ was determined using the TdT in situ apoptosis kit (DAB TUNEL-based Apoptosis Detection Assay; R&D Systems, Minneapolis, MN). The murine embryonic fibroblasts (MEFs) were produced as previously described (Albanese *et al.*, 1999) and cultured following the 3T3 protocol. The expression plasmids for adenovirus Cre (Ad-Cre) or control (Ad-Null) were previously described (Wang *et al.*, 1995). The rat *c-jun* was subcloned in murine sarcoma cytomegalovirus (MSCV)-internal ribosome entry site (IRES)-green fluorescent protein (GFP) to form MSCV-*c-jun*-IRES-GFP.

Reagents and Antibodies

The following reagents and antibodies were used: H_2DCFDA (Invitrogen, Carlsbad, CA); anti-Cre (EMD Biosciences, San Diego, CA); anti-*c-jun* (H-79), anti-survivin, and anti-rho-guanine nucleotide dissociation inhibitor (GDI; Santa Cruz Biotechnology, Santa Cruz, CA); VDAC-1 (Abcam, Cambridge, MA); and DAPI (4′,6′-diamino-2-phenylindole; Sigma-Aldrich, St. Louis, MO). Amplex Red H_2O_2 detection kit was from Invitrogen. Reagents and their final concentration used in experiments were *N*-acetyl-L-cysteine (NAC; 5 mM), diphenyleneiodonium chloride (DPI; 10 μM), ammonium pyrrolidinedithiocarbamate (PDTC; 10 μM), rotenone (1 μg/ml), and H_2O_2 were purchased from Sigma-Aldrich. Measurements of H_2O_2 production were conducted using Amplex Red Hydrogen Peroxide/Peroxidase Assay Kit from Invitrogen (Mishin *et al.*, 2010). Catalase activity was determined using the Catalase Assay Kit from Caymen Chemicals (Ann Arbor, MI; Sinha, 1972), and the In Gel MnSOD activity was done as previously described (Beauchamp and Fridovich, 1971).

Cell Culture, Viral Cell Transduction, and Reporter Gene Assays

Cells were maintained under standard tissue culture conditions in DMEM supplemented with 10% FBS and 100 mg/ml each of penicillin-streptomycin at 37°C with 5% CO_2. Adenovirus propagation was previously described (Wang *et al.*, 2003). Infection was done at a multiplicity of infection (MOI) of 50, cells were cultured overnight, and media were changed before experimental analysis. Retroviral infections were conducted as previously described (Wang *et al.*, 2003). Transfections were conducted using Genejuice transfection reagent (EMD Biosciences, San Diego, CA) as described (Bouras *et al.*, 2005). Statistical analysis was conducted using the Mann-Whitney U test.

Immunofluorescence and Confocal and Electron Microscopy

c-jun$^{f/f}$ cells were grown on chamber slides and then treated with either Ad-Null or Ad-Cre. Cells were then stained with antibodies against cre-recombinase and *c-jun*, and DAPI was used as nuclear stain. The microscopic images were captured using the 20× and 63× objectives of an Olympus LSM-5 Meta laser confocal scanning microscope (Olympus America, Center Valley, PA). Briefly, confluent *c-jun*$^{f/f}$ cells treated with adenoviruses were harvested and washed with PBS. Cells were fixed in paraformaldehyde and permeabilized with Triton X-100, followed by a PBS wash, and were stained with primary antibodies and consequently with fluorophore-tagged secondary antibodies.

For electron microscopy (EM) virus-treated cells were plated on fibronectin-coated glass coverslips and grown to approximately 80% confluence. The cells were then rinsed with PBS and fixed in 2.5% glutaraldehyde/0.1 M for 2 hr at room temperature, postfixed in 1% osmium tetroxide for 1 hr, en bloc stained with uranyl acetate, and processed in situ for conventional electron microscopy araldite embedding procedure. Layers of plastic-embedded cells were removed from the coverslips, re-embedded in plastic, and ultrathin sections were cut parallel to the original plane of the coverslip. Sections were then poststained with uranyl acetate and lead citrate, and observed and photographed with a Hitachi H-7600 transmission electron microscope (Hitachi, Tokyo, Japan).

Assessment of ROS Production

H_2DCFDA staining for ROS was performed on fibroblasts treated with Ad-Null and Ad-Cre according to the manufacturer's instructions. DCFDA, at 5 mM, was used for staining the cells for 30 min, followed by fluorescence-activated cell sorting (FACS) sorting of stained cells at excitation and emission wavelengths of 492–495 and 517–527 nm, respectively. H_2DCFDA is a cell-permeant indicator for ROS that is nonfluorescent until the acetate groups are removed by intracellular esterases and oxidation occurs within the cell.

Assays for Assessment of Cellular Apoptosis

FACS-based cell cycle assays were performed using propidium iodide staining of the virus-treated cells in citrate buffer. Assays of cellular apoptosis were performed using annexin V staining on living cells using the annexin V kit from BD Biosciences (San Jose, CA) followed by the FACS sorting of fluorescent apoptotic cells.

Real-Time PCR and ELISA

All gel-based and real-time quantitative RT-PCR (qRT-PCR) assays were performed as previously described (Katiyar *et al.*, 2007). Briefly, RNA extracted using standard GITC method was RQ1 DNase I (Promega, Madison, WI) treated, phenol-chloroform extracted, and quantitated using a Nanodrop spectrophotometer (Nanodrop Tech, Wilmington, DE). An equal quantity of RNA from each sample was reverse-transcribed using Iscript Reverse transcriptase (Bio-Rad, Hercules, CA). Primers for all the genes and gene transcripts including housekeeping control genes and gene transcripts are listed in Table 1.

Laser Capture Microdissection

Mammary glands from the following bitransgenic mice genotypes: wild-type (cre^{+}/*c-jun*$^{wt/wt}$; resulting genotype: *c-jun*$^{+/+}$), heterozygotes (cre^{+}/*c-jun*$^{f/w}$; resulting genotype: *c-jun*$^{+/-}$), or knockouts (cre^{+}/*c-jun*$^{f/f}$; resulting genotype: *c-jun*$^{-/-}$) were frozen in optimal temperature compound on dry ice. The frozen tissue blocks were trimmed and cryosectioned at −20°C in a cryostat machine onto cold, RNase-free sterile glass slides. Each slide was mounted in the LCM machine, and ~200–1000 mammary epithelial cells were picked by firing lasers on to the resin-bearing caps. RNA was isolated using microRNAeasy RNA extraction kits (Qiagen, Valencia, CA) followed by DNase treatment and concentrated in a small volume using DNA-free kit (Zymo Research, Orange, CA). RNA quantity and quality was measured in a Nanodrop 1000 spectrophotometer. This RNA was then subjected to hybridization to Affymetrix RNA chips (Santa Clara, CA) for assessing the relative expression of genes affected by *c-jun* excision.

Gene Expression Arrays and Pathways Analysis

RNA samples extracted from laser capture microdissected mammary epithelial cells from wild-type *c-jun*$^{+/+}$ and knockout *c-jun*$^{-/-}$ bitransgenic mice mammary glands were processed for Affymetrix 430 2.0 arrays to determine gene expression. RNA quality was determined by gel electrophoresis. Probe synthesis and hybridization were performed as previously described (Li *et al.*, 2008). Analysis of the arrays was performed using the R statistics package (www.r-project.org) and the limma library of the Bioconductor software package (www.bioconductor.org). Arrays were normalized using robust multiarray analysis, and a p of 0.05 was applied as statistical criterion for differ-

Table 1. List of oligonucleotide primers used in PCR, RT-PCR, real-time qRT-PCR analysis, and chromatin immunoprecipitation assays

Gene	Orientation	Sequence 5′→3′
c-jun genotyping	Forward	CTC ATA CCA GTT CGC ACA GGC GGC
	Reverse	CCG CTA GCA CTC ACG TTG GTA GGC
	Reverse	CAG GGC GTT GTG TCA CTG AGC T
RPL-19 (DNA PCR)	Forward	AAT GCT CGG ATG CCT GAG AA
	Reverse	CTC CAT GAG GAT GCG CTT GT
Cre recombinase	Forward	TGC TCT GTC CGT TTG CCG
	Reverse	ATC GTG TCC AGA CCA GGC
RPL-19 (for RT-PCR)	Forward	CTG AAG GTC AAA GGG AAT GTG
	Reverse	GGA CAG AGT CTT GAT GAT CTC
c-jun (for RT-PCR)	Forward	AGA GCG GTG CCT ACG GCT ACA GTA A
	Reverse	CGA CGT GAG AAG GTC CGA GTT CTT G
MnSOD	Forward	GCA CAT TAA CGC GCA GAT CA
	Reverse	AGC CTC CAG CAA CTC TCC TT
CuZnSOD	Forward	AAG GCC GTG TGC GTG CTG AA
	Reverse	CAG GTC TCC AAC ATG CCT CT
GPX	Forward	CCT CAA GTA CGT CCG ACC TG
	Reverse	CAA TGT CGT TGC GGC ACA CC
Catalase	Forward	GCA GAT ACC TGT GAA CTG TC
	Reverse	GTA GAA TGT CCG CAC CTG AG
Rac 1	Forward	CTG CCT GCT CAT CAG TTA CACG
	Reverse	GGA CAG AGA ACC GCT CGG ATA
Rac 2	Forward	CAG GTC AGG AGG ACT ATG ACC G
	Reverse	GAT TGC CTC ATC GAA GAC GGT
p40phox	Forward	CAA AGT CTA CAT GGG CGC AAA
	Reverse	TGT CTT CAT AGA AGT AGC ATC GTA GCC
p67phox	Forward	CTA TCT GGG CAA GGC TAC GGT T
	Reverse	CAC AAA GCC AAA CAA TAC GCG
gp91phox	Forward	AGT CGG GAT TTC TGA CCG GTA T
	Reverse	TCC AGT CTC CAA CAA TAC GGA TAT G
18S r-RNA	Forward	AGG AAT TCC CAG TAA GTG CG
	Reverse	GCC TCA CTA AAC CAT CCA A
AP-1 elements	Forward	AGA AGT GAG TGG ATG TGA TGC CCA
	Reverse	AGT ACA TCG TTG ACT GCA CGA CCT
Negative (4)	Forward	TTC ATT TGC TGT CTG TCA CCG GG
	Reverse	TGC AGA TAG TCC CAG CAT TGG GTA
Oligos used for creating AP-1 deletion in MnSOD promoter constructs	Forward	CAG GGC ATA AAT TAA GAA GGC CCC TG
	Reverse	CAG GGG CCT TCT TAA TTT ATG CCC TG

entially expressed genes (Zhou *et al.*, 2010). These genes were then grouped using hierarchical clustering with "complete" agglomeration. Expression profiles are displayed using Treeview (http://taxonomy.zoology.gla.ac.uk/ROD/treeview.html). Classification and clustering for pathway level analysis used ASSESS (Analysis of Sample Set Enrichment Scores) (Edelman *et al*, 2006).

RNA amplification was performed from 5 ng of total RNA followed by cDNA production and its purification using a DNA cleaning kit from Zymo Research. The purified cDNA was then quantified on a Nanodrop ND-1000 Spectrophotometer (Thermo Scientific, Waltham, MA) and 5 μg of amplified cDNA was fragmented and chemically labeled with biotin to generate biotinylated cDNA using FL-Ovation cDNA biotin labeling module V2 (NuGen Technologies, San Carlos, CA).

Low-Density Apoptosis Arrays

The cDNA prepared from purified RNA extracted *c-jun*$^{f/f}$ fibroblasts treated with either adenovirus null (wild type [WT]) or adenovirus expressing cre-recombinase (knockout [KO]) was amplified on prefabricated, low-density, 384-well apoptosis arrays and run according to the manufacturer's instructions (SA Bioscience, Gaithersburg, MD).

RESULTS

Endogenous c-jun *Inhibits Signaling Pathways Promoting Apoptosis In Vivo*

c-jun has been shown to either inhibit or induce cellular apoptosis in different cell types (Seaman, 1976; Udou *et al.*, 2004; Vleugel *et al.*, 2006; Hettinger *et al.*, 2007; Podar *et al.*, 2007). We conducted studies to determine the role of endogenous *c-jun* in mammary epithelial cell survival. Because *c-jun* somatic deletion is embryonically lethal, we intercrossed floxed *c-jun* (*c-jun*$^{f/f}$) transgenic mice with MMTV-Cre mice and conducted LCM of mammary epithelial cells from mouse mammary glands (*Materials and Methods*; Figure 1A). mRNA derived from mammary epithelial cells of six separate transgenic mice was subjected to microarray analysis and subsequently to pathways analysis using ASSESS (Figure 1A). Gene expression pathways and the induction of apoptosis associated with ROS production were induced upon *c-jun* deletion (Figure 1A). To examine whether *c-jun* deletion–regulated expression of specific pro- or antiapoptotic genes, we conducted RT-PCR–based expression analysis of 87 genes (using low-density apoptosis arrays) previously shown to be involved in apoptosis. Thirty-nine proapoptotic genes were induced, and 16 anti-apoptotic genes were repressed upon deletion of *c-jun* (Figure 1B). The relative change in gene expression of the antiapoptotic and proapoptotic genes are shown on a log scale (Figure 1C). Deletion of *c-jun* induced expression of apoptotic genes and reduced expression of anti-apoptotic genes (Figure 1C). The inhibitor of apoptosis protein (IAP) BIRC5 (survivin) was repressed substantially upon deletion of endogenous *c-jun* (Figure 1C). RT-PCR–based analysis of *c-jun* gene expression within laser capture–microdissected mammary epithelial cells derived from Cre recombinase expressing bitransgenic mammary glands also showed reduction in *c-jun* expression (Figures 1D).

To determine whether the excision of *c-jun* within the mammary epithelial cells had affected mammary gland development and mammary ductal morphology, we performed mammary gland whole-mount analyses. Mammary glands squashes prepared by staining the entire #4 mammary glands from cre^{+}/c-jun$^{f/f}$ (resulting genotype: *c-jun*$^{-/-}$ or KO) and cre^{+}c-jun$^{f/w}$ (resulting genotype: *c-jun*$^{+/-}$) to littermate controls cre^{+}/c-jun$^{wt/wt}$ (resulting genotype: *c-jun*$^{+/+}$ or WT) were photographed and carefully compared (Supplemental Figure 1A). The morphological structure and architecture was unchanged between genotypes. Mammary gland ductal branching complexity number was also largely unaltered (Supplemental Figure 1A). Studies of the cellular components of the mammary gland of the mice were next conducted. The relative

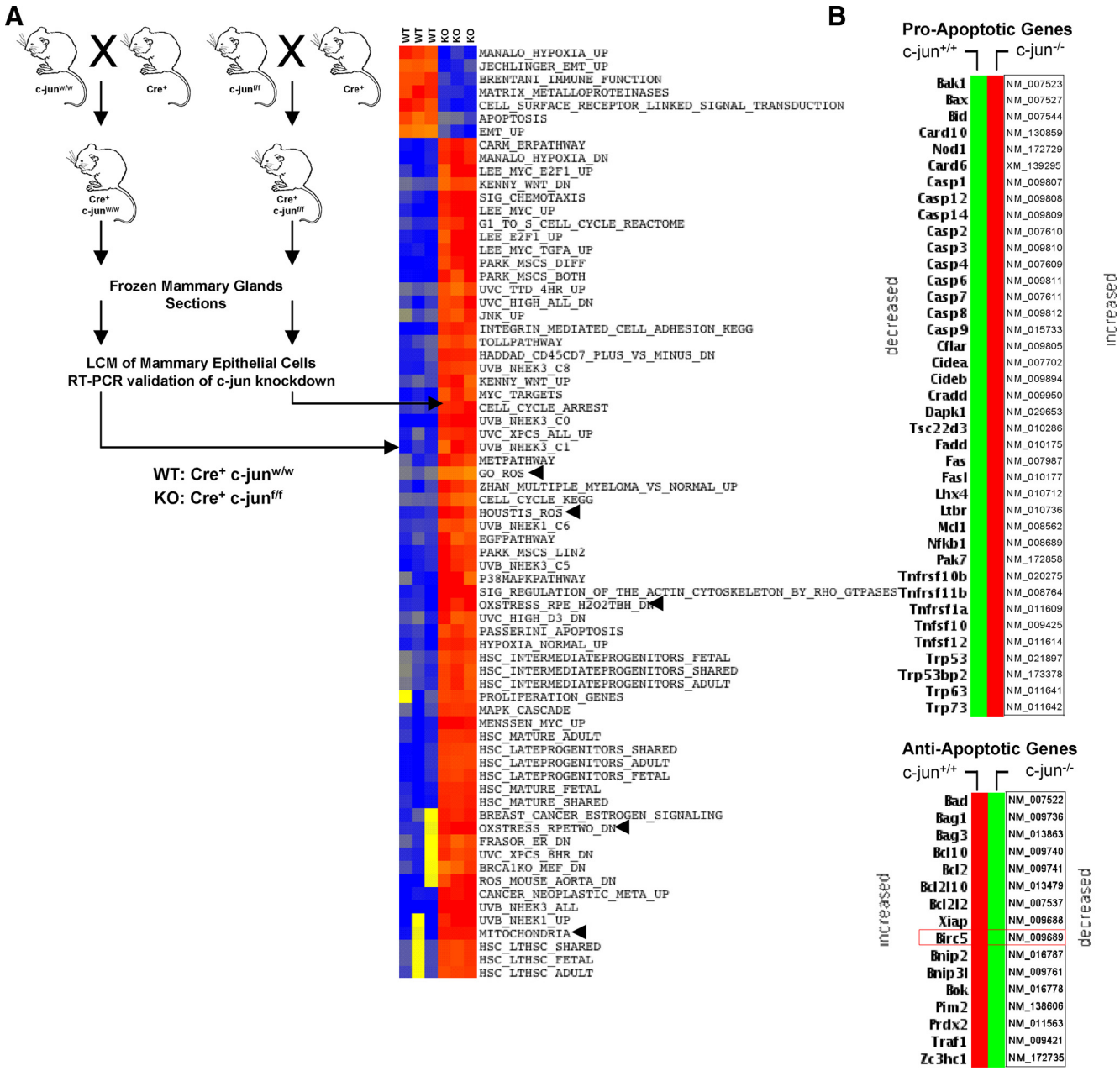

Figure 1. Endogenous *c-jun* represses gene expression pathways governing cellular apoptosis and ROS production in vivo. (A) Schematic representation of intercrosses between MMTV-Cre and *c-jun*$^{f/f}$ transgenic mice performed to produce *c-jun*$^{+/+}$ and *c-jun*$^{-/-}$ mice. The mammary glands from these mice were subjected to laser capture microdissection (LCM) to enrich and purify mammary epithelial cells for performing microarray-based gene expression analysis. ASSESS pathway analysis was performed on the differentially expressed genes. The blue gradient coloration in the heat map shows down-regulation of the indicated pathways, whereas red depicts up-regulation of those pathways. (B) Heat map of differentially expressed pro- and antiapoptotic gene transcripts up- or down-regulated upon treatment of floxed *c-jun* cells with Ad-Null or Ad-Cre. (C) Scatter plot for the gene expression profiling performed using low-density apoptosis qRT-PCR arrays indicating expression of pro- and antiapoptosis genes, with the direction of gene expression show by red (up-regulated) and green (down-regulated) genes.

number of cells per field and the area covered by cells lining mammary glands were carefully assessed and characterized by pixels per field and demonstrated ~50% reduction in the number of epithelial cells observed per field and the same for their area. (Supplemental Figure 1B).

Endogenous c-jun *Inhibits ROS Production via Mitochondrial Complex I and NOX1*

To determine the role of endogenous *c-jun* in ROS production, *c-jun*$^{fl/fl}$ MEFs (Figure 2A) were transduced with an adenoviral expression vectors encoding cre (Ad-Cre) or a control vector (Ad-Null). The excision of *c-jun* was documented by RT-PCR analyses for *c-jun* mRNA normalized to the internal control Rpl-19 and deletion of the floxed site by PCR (Figure 2AIII). ROS production was visualized by 2′7′-dichlorofluorescein diacetate (DCFDA) and quantitated by FACS sorting (Figure 2, B and C), which demonstrated an approximate doubling of DCFDA positivity (Figure 2B). Confocal microscopy combining staining of mitochondria with mitotracker dye evidenced a colocalization of DCFDA

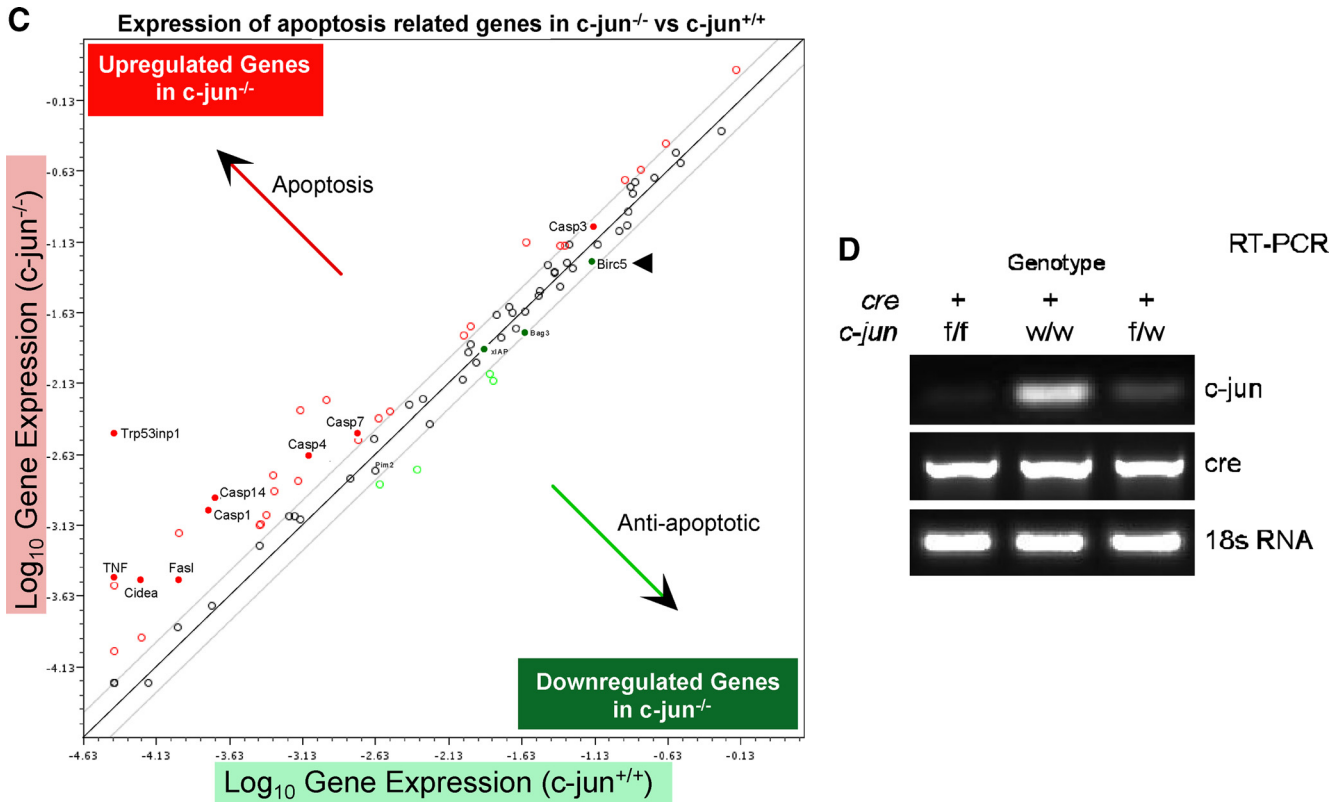

Figure 1. *Continued.*

with mitochondria (yellow; Figure 1C). Additional nonmitochondrial DCFDA was also seen. Reintroduction of *c-jun* by retroviral transduction into *c-jun*$^{-/-}$ cells reversed the increase in DCFDA positivity by FACS (data not shown). To examine further the source of endogenous ROS repressed by *c-jun*, ROS inhibitors were used. NAC and PDTC had been thought to act as antioxidants. PDTC inhibits IκB-ubiquitin ligase activity (Hayakawa *et al.*, 2003). Rotenone, is an inhibitor of the mitochondrial electron transport chain, and DPI is an inhibitor of the NOX enzymes that are the major mediators of nonmitochondrial ROS (Kamata and Hirata, 1999). Addition of DPI, PDTC, or rotenone reduced DCFDA fluorescence (Figure 2D) suggesting both NOX- and mitochondrial-dependent sources of ROS in *c-jun*$^{-/-}$ cells.

Endogenous c-jun *Maintains Mitochondrial Membrane Potential*

Apoptosis assessed by annexin V staining was increased fourfold in *c-jun*$^{-/-}$ cells (Figure 3A). EM of the mitochondria demonstrated mitochondrial blebbing (Figure 3B) characteristic of apoptotic cell death. The size of mitochondria assessed by mitotracker staining was unchanged in *c-jun*$^{-/-}$cells (Figure 3C). The mitochondrial membrane potential (Dym) regulates ROS formation and efflux. O_2^- production increased the number of cells with medium and low Dym. Quantitation of JC-1 staining was conducted to measure Dym and demonstrated a 3–5-fold increase in staining in *c-jun*$^{-/-}$ cells (Figure 3D).

To determine the role of c-Jun and c-Jun–regulated ROS in cellular growth and apoptosis, cellular proliferation assays were conducted. *c-jun*$^{-/-}$ MEFs have a severe proliferative defect that can be passaged only a few times before entering premature senescence. To avoid any independent effects of serial passage and senescence, the studies were conducted acutely on early-passage MEFs. *c-jun*$^{f/f}$ cells were transduced with an adenovirus expressing cre via an IRES to the GFP protein (Supplemental Figure 3A). Immunohistochemical staining confirmed cells transduced with Cre lacked c-Jun protein. GFP-positive cells were selected and analyzed. *c-jun*$^{-/-}$ MEFs demonstrated a reduced proliferation rate assessed by cellular counting (Supplemental Figure 3A) or by MTT assays (Supplemental Figure 3B). *c-jun*$^{-/-}$ MEFs displayed enhanced sensitivity to H_2O_2-induced apoptosis (Supplemental Figure 3C).

c-jun*–dependent ROS Production Governs MnSOD, Catalase, and GPX Expression*

We examined further the mechanisms governing endogenous *c-jun*–mediated inhibition of ROS production. Increased ROS production in the *c-jun*$^{-/-}$ cells may be a consequence of either reduced ROS elimination or increased ROS production. O_2^- is converted to H_2O_2 by matrix manganese superoxide dismutase (MnSOD; Temkin and Karin, 2007), whereas catalase and GPX either separately or synergistically convert H_2O_2 to H_2O. To determine the mechanism by which *c-jun* inhibited ROS production, we examined the role of *c-jun* in regulating MnSOD and catalase abundance. We examined the abundance of MnSOD by quantitative real-time RT-PCR upon acute excision of *c-jun* using Ad-Cre. As endogenous *c-jun* mRNA levels decreased (Figure 4AI), MnSOD mRNA transcript abundance increased (Figure 4AII). O_2^- released to the mitochondrial intramembrane space is dismutated by CuZnSOD (Okado-Matsumoto and Fridovich, 2001). ROS are further detoxified by GPX (Nohl and Jordan, 1980), which uses GSH in catalysis. The relative abundance of MnSOD, CuZnSOD, catalase, and GPX

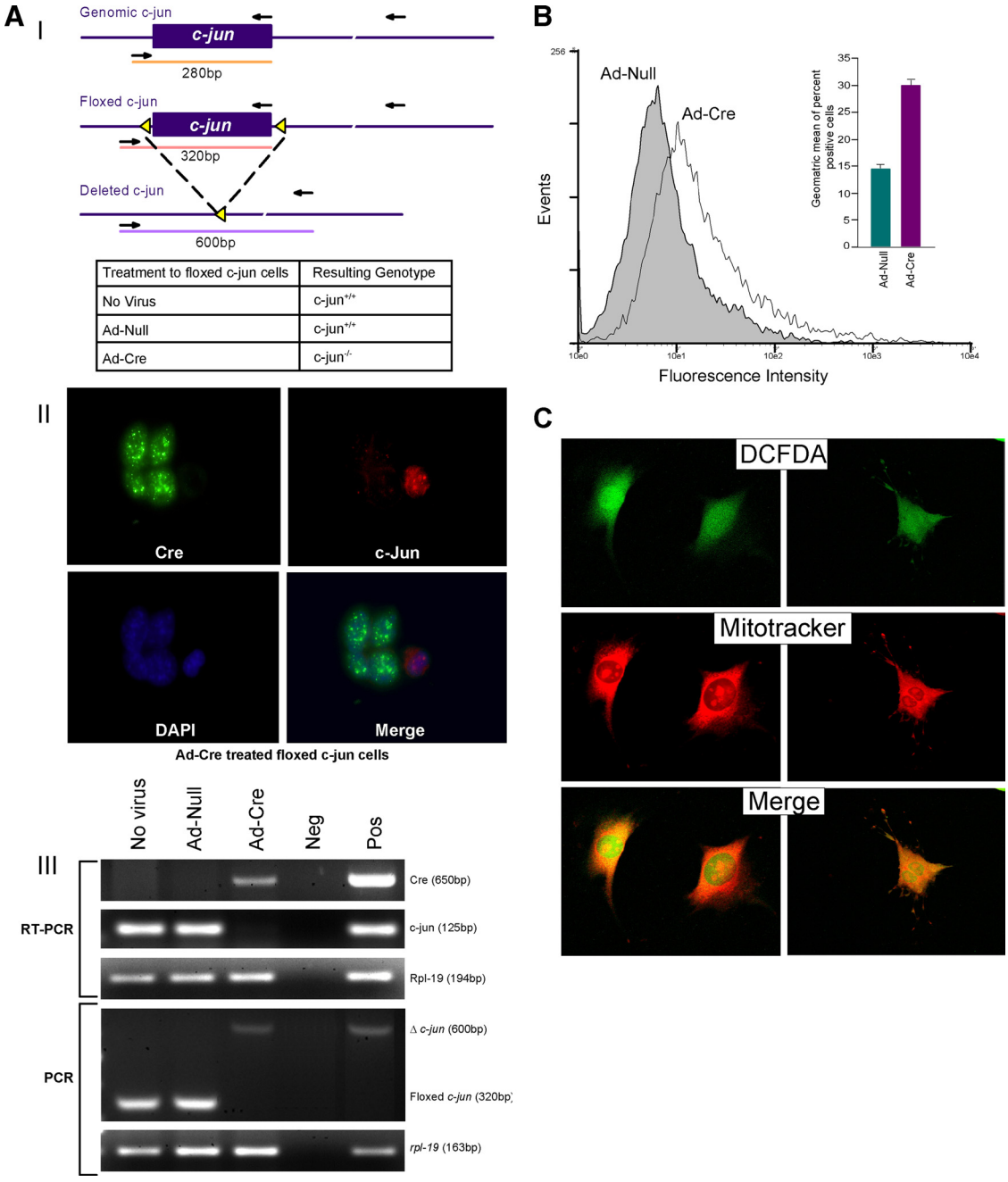

Figure 2. Somatic excision of *c-jun* induces mitochondrial and NOX1-dependent ROS production. (AI) Schematic diagram of the genomic wild-type (*c-jun*), floxed (*c-jun*$^{f/f}$), and deleted *c-jun* (*c-junP*$^{\Delta}$) locus with loxP sites (◀) and PCR primer binding sites (→). Adenovirus treatments to floxed *c-jun* cells, and resulting cellular genotypes. (II) Confocal microscopic images of Ad-Cre–treated *c-jun*$^{f/f}$ fibroblasts showing expression of Cre-recombinase and *c-jun*. DAPI-stained nuclei. Note that the cells expressing Cre have lost *c-jun* expression. (III) RT-PCR showing expression of cre-recombinase, *c-jun*, and *rpl-19* (housekeeping gene control) mRNA transcripts in RNA from no virus NS Ad-Null– and Ad-Cre–treated *c-jun*$^{f/f}$ fibroblasts. PCR genotyping of DNA from no virus and Ad-Null– and Ad-Cre–treated *c-jun*$^{f/f}$ cells showing floxed and excised *c-jun* alleles. (B) FACS-based quantification of DCFDA-stained ROS production in Ad-Null– and Ad-Cre–treated floxed *c-jun* cells (data are mean ± SEM). (C) High-resolution confocal microscopic images of the DCFDA staining of intracellular ROS in Ad-Cre–treated floxed *c-jun* cells. Mitotracker mitochondrial stain was used for visualization of mitochondria (data are mean ± SEM). (D) DCFDA staining of Ad-Null– or Ad-Cre–treated fibroblasts after addition of various ROS inhibitors.

were assessed upon acute deletion of *c-jun* to determine the role of endogenous *c-jun* in regulating the key components involved in eliminating ROS (Figure 4A, III–V). Quantitative RT-PCR transcript analysis was conducted, and mean data of multiplicate studies demonstrated that *c-jun* excision induced MnSOD 2.5-fold. More modest changes occurred with catalase and GPX (1.5- to 2-fold). CuZnSOD mRNA expression was unchanged (Figure 4A, III–V). The finding that MnSOD mRNA increased and CuZnSOD was unchanged upon excision of *c-jun* in fibroblasts was confirmed by microarray analysis of the *c-jun*$^{-/-}$ mammary gland in which MnSOD was increased

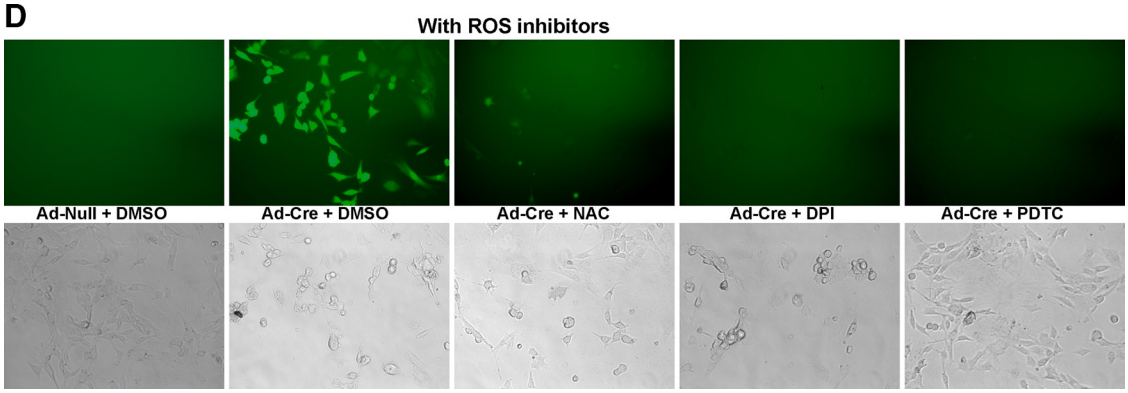

Figure 2. *Continued.*

(1.6-fold, mean of n = 3), and CuZnSOD mRNA abundance was unchanged.

We had previously shown that ROS induces MnSOD expression (Tanaka *et al.*, 2002). We therefore examined

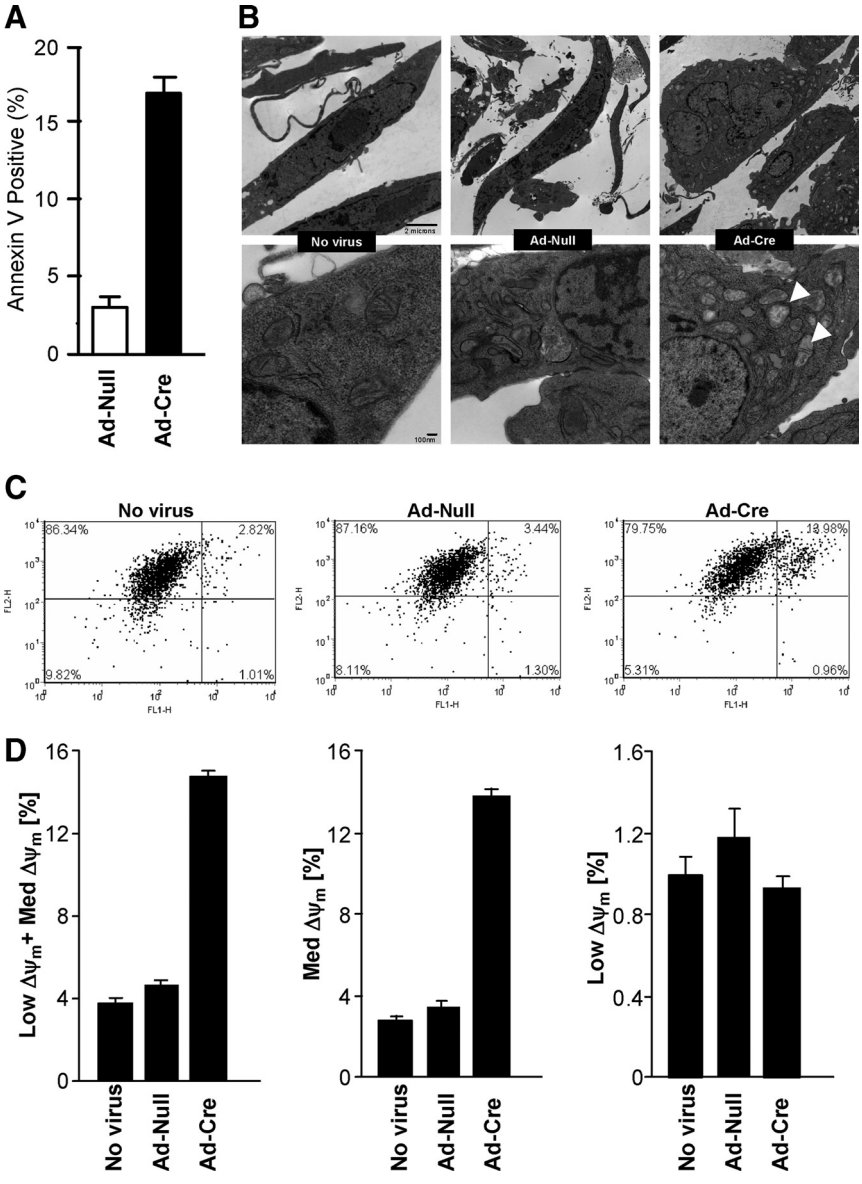

Figure 3. c-*jun* determines mitochondrial membrane potential and apoptosis. (A) Annexin V staining for assessment of apoptotic cells after *c-jun* excision (data are mean ± SEM for n > 5). (B) Electron micrographs of the floxed *c-jun* cells with (No virus or Ad-Null) or without *c-jun* expression (Ad-Cre). (C) Mitochondrial membrane potential measurements using JC-1 mitochondrial probe after *c-jun* excision (data are mean ± SEM). (D) Quantitation of JC-1 staining and measurement of Dym, indicating a 3–5-fold increase in staining in *c-jun*$^{-/-}$ cells.

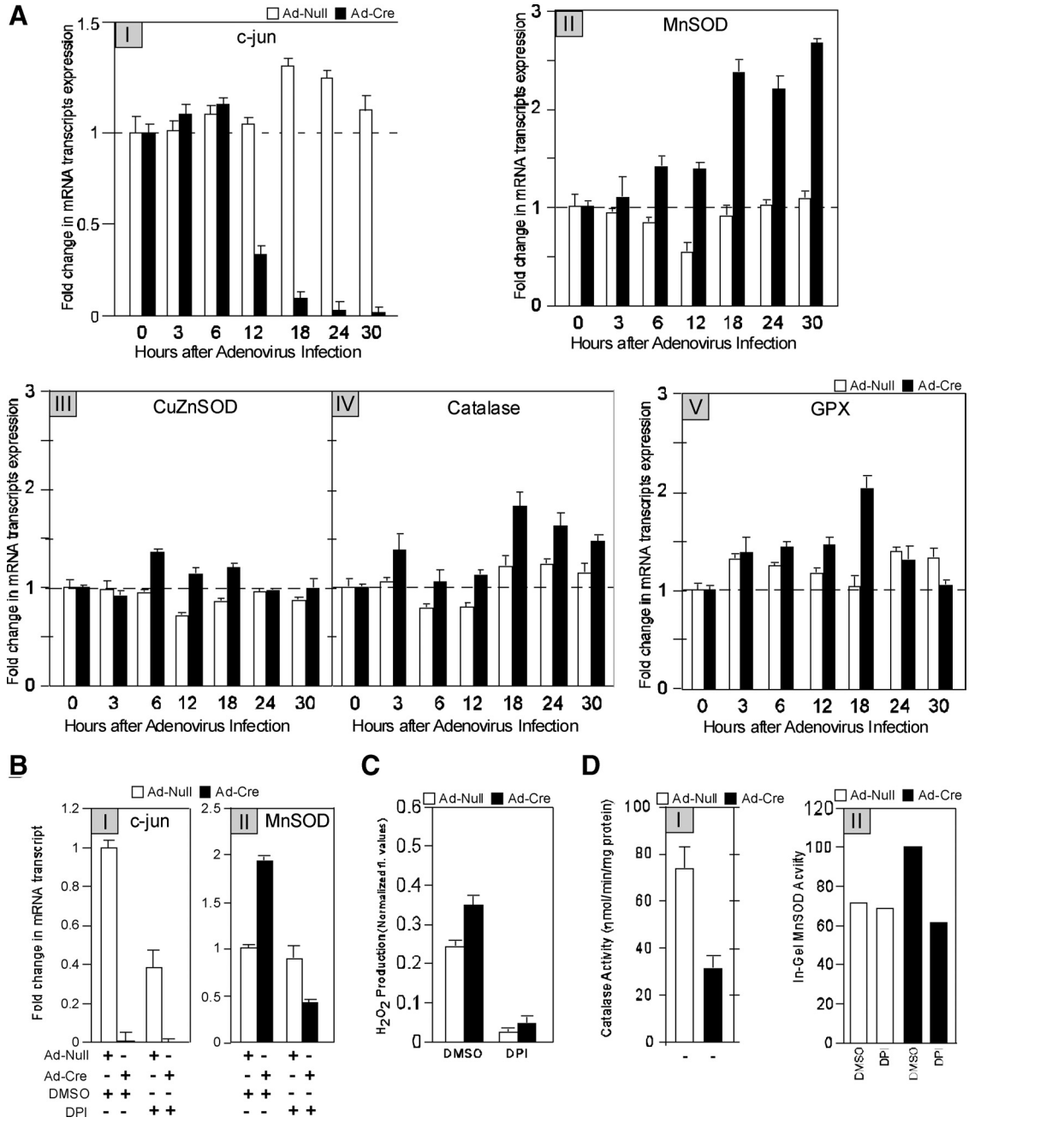

Figure 4. c-*jun* excision induces MnSOD expression via a ROS-dependent mechanism. (A) qRT-PCR–based assessment of expression of *c-jun* (I), MnSOD (II), CuZnSOD (III), catalase (IV), and GPX (V) transcripts at various time points after treatment of floxed *c-jun* cells with Ad-Null or Ad-cre to excise the *c-jun* gene. The real-time qRT-PCR expression data for various targets were normalized to amplification of 18S rRNA housekeeping gene control in every sample. (B) Expression of *c-jun* and MnSOD transcripts after treatment of Ad-Null– or Ad-Cre–treated floxed *c-jun* cells with the ROS inhibitor DPI. (C) Quantitation of H_2O_2 levels after *c-jun* excision and DPI treatment. (D) Catalase enzyme activities and (E) MnSOD enzyme activity in Ad-Null– or Ad-Cre–treated floxed *c-jun* cells in the presence of various ROS inhibitors (data are mean ± SEM).

whether inhibition of ROS production in *c-jun*$^{-/-}$ cells was responsible for the increase in MnSOD. The addition of DPI (Figure 4B), rotenone, or PDTC (not shown) reversed the hyperactivation of MnSOD. Thus, increased ROS from NOX1 and mitochondrial sites produced in *c-jun*$^{-/-}$ cells enhances MnSOD expression. Consistent with an important role for MnSOD in converting O_2 to H_2O_2, H_2O_2 production (Figure 4C) was reduced by DPI. Consistent with the induction of expression in *c-jun*$^{-/-}$ cells, MnSOD enzyme activity was also increased in *c-jun*$^{-/-}$ cells (Figure 4D). The induction of MnSOD activity in *c-jun*$^{-/-}$ cells was reduced by DPI (Figure 4D). To determine whether the increase in H_2O_2 abundance in *c-jun*$^{-/-}$ cells was due to reduced catalase activity, catalase activity assays were conducted. Catalase activity was reduced by 60% upon deletion of *c-jun* (Figure 4D). The reduction in catalase activity was partially reversed by DPI, suggesting NOX-dependent ROS are a source of reduced catalase activity in *c-jun*$^{-/-}$ cells.

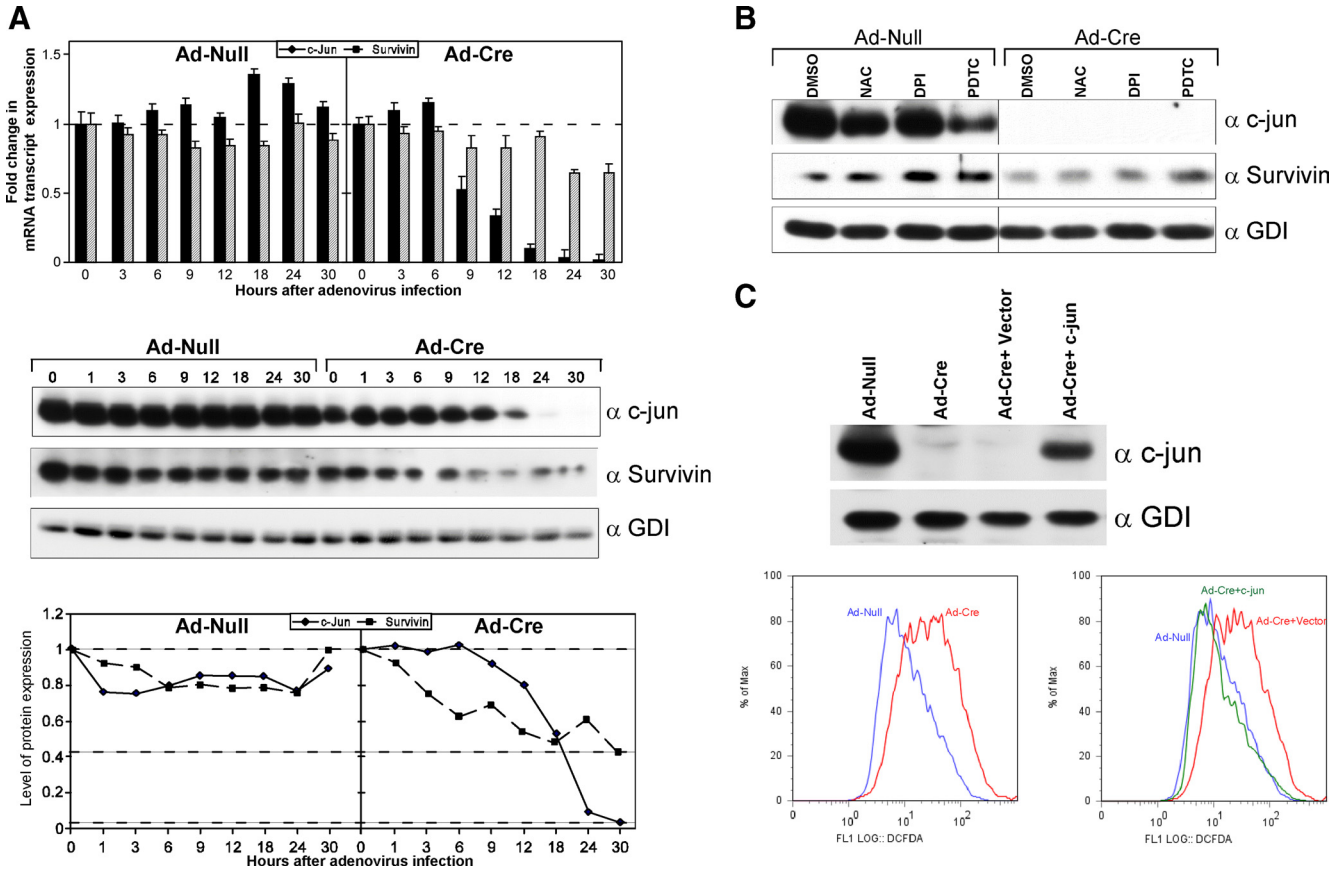

Figure 5. Endogenous *c-jun* maintains survivin abundance. (A) mRNA and protein abundance for *c-jun* and survivin determined after acute excision of *c-jun* using Ad-Cre treatment of *c-jun*$^{fl/fl}$ cells quantitated by RT-PCR (data are mean ± SEM for n > 5). (B) Western blot analysis of surviving abundance in wild-type versus *c-jun*$^{-/-}$ cells after treatment with ROS inhibitors for 24 h as indicated. (C) Western blot and DCFDA analysis of *c-jun*$^{-/-}$ cells transduced with retrovirus encoding *c-jun*. *c-jun* restores endogenous *c-jun* levels and reverses the increased production of ROS.

Endogenous c-jun *Induces Survivin (BIRC5) in Part via ROS*

Microarray and RT-PCR analysis of mRNA from LCM of the mammary epithelial cell targeted MMTV-Cre/*c-jun*$^{fl/fl}$ bitransgenics demonstrated a reduction in the abundance of several antiapoptotic genes (Figure 1, B and C). The abundance of BIRC5 (survivin), in particular, was down-regulated. To determine whether BIRC5 was also a direct target of endogenous *c-jun*, acute excision of *c-jun* was conducted and BIRC5 abundance was determined (Figure 5A). *c-jun* excision was associated with a decrease in BIRC5 (survivin) mRNA (by RT-PCR) and protein levels. Survivin abundance in *c-jun*$^{-/-}$ cells was reduced in part by the addition of ROS inhibitors (Figure 5B). DPI and PDTC treatment increased survivin abundance in *c-jun*$^{-/-}$ cells 3–5-fold (Figure 5B, lanes 5 vs. 7 and 8). Reintroduction of *c-jun* restored *c-jun* and survivin levels and reversed aberrant ROS production (Figure 5C).

Collectively these studies demonstrate acute *c-jun* excision increased proapoptosis and inhibited antiapoptotic gene expression in vivo. The mammary epithelium in vivo *c-jun* excision or *c-jun*$^{fl/fl}$ cultured cells induced expression of genes that catalase ROS, mitochondrial membrane potential and both mitochondrial and NOX-based ROS, which induced MnSOD, and catalase expression. The inhibition of ROS production by endogenous *c-jun* reduced cellular apoptosis and promoted contact-independent growth. Because *c-jun* functions as a pivotal downstream regulator of diverse biological processes governing cellular proliferation and growth, these studies provide a direct link between *c-jun* and mitochondrial function.

DISCUSSION

The current studies demonstrate an essential role for endogenous *c-jun* in maintaining mammary epithelial cellular survival in vivo. Double transgenic mice (*c-jun*$^{fl/fl}$-MMTV-Cre) and conditional knockout MEFs were generated to identify the key signaling pathways regulated by endogenous *c-jun* in vivo. Genome-wide expression studies conducted of mRNA derived from laser capture–microdissected mammary epithelium from these double transgenic mice identified the key pathways regulated by endogenous *c-jun*. In the mammary epithelium and fibroblasts the key pathways regulated by endogenous *c-jun* govern cellular apoptosis and ROS production. RT-PCR analysis of 87 genes confirmed that 39 apoptotic genes were induced and 16 antiapoptotic genes were repressed upon deletion of *c-jun*.

Herein, acute *c-jun* excision increased apoptosis. The induction of cellular senescence, which occurs upon several cellular divisions, is associated with the induction of p53/p21^{CIP1} (MacLaren *et al.*, 2004). To distinguish the effects of *c-jun* excision from the effects of cellular senescence the molecular events, accompanying acute somatic excision of

c-jun were characterized. The apoptosis induced upon acute excision of *c-jun* herein was associated with increased annexin V staining, characteristic of phosphatidyl-serine exposure on the cellular membrane seen in apoptosis and features of caspase 3 cleavage and activation (Supplemental Data) indicative of the intrinsic mitochondrial pathways of apoptosis. Mitochondrial morphology reflected the characteristic feature of mitochondrial cristae swelling and inner mitochondrial membrane swelling.

The current studies define a central role for endogenous *c-jun* gene in maintaining ROS homeostasis. The decreased membrane potential of *c-jun*$^{-/-}$ cells would be anticipated to increase ROS production and enhance efflux (Tirosh *et al.*, 2003). Acute *c-jun* excision enhanced ROS production and expression of the enzymes that catalase and detoxify ROS (MnSOD and GPX). The induction of gene expression occurred within 16–18 h. The induction of the cellular ROS-catalyzing enzymes was accompanied by a decrease in mitochondrial membrane potential. ROS are known to induce expression of MnSOD (Tanaka *et al.*, 2002). The enhanced production of MnSOD in *c-jun*$^{-/-}$ cells was abolished by addition of DPI, indicating that ROS production from mitochondrial complex I and NOX are inhibited by endogenous *c-jun*. Thus, endogenous *c-jun* inhibits MnSOD production via NOX1 and mitochondrial complex 1.

Apoptosis is regulated via extrinsic pathways that are triggered by ligand binding, whereas the intrinsic apoptotic pathways involves mitochondria, which release cytochrome *c* that binds and activates Apaf1 (apoptotic protease activation factor 1). Apaf1 induces assembly of the apoptosome, leading to activation of caspase 9 members of the IAP family including survivin and others (ML-IAP, XIAP, $CIAP_1$, $CIAP_2$, NIAP, and Apollon). These factors block apoptosis downstream of cytochrome *c* release by interfering with caspase 9 activity and processing and inhibiting the terminal effectors caspase-3 and -7. Increased ROS production has been linked to cellular apoptosis through sustained JNK activation and an additional pathway (Kamata *et al.*, 2005; Chang *et al.*, 2006) that is inhibited by a prosurvival NFκB (nuclear factor κB) pathway (Temkin and Karin, 2007). The current studies extend these prior observations by demonstrating that the endogenous *c-jun* functions to inhibit ROS production (Supplemental Figure 3). The IAP BIRC5 (survivin) was reduced upon deletion of *c-jun*. Survivin is a 16.5-kDa protein, with a single baculovirus IAP repeat (BIR). Mitochondrial survivin orchestrates a novel pathway of apoptosis inhibition, which contributes to tumorigenesis (Dohi *et al.*, 2004). On deletion of *c-jun*, ROS levels rise, and survivin and other apoptotic gene levels fall, inducing apoptosis (Supplemental Figure 3). *c-jun* induced survivin abundance in a ROS-dependent manner. ROS generated independently of *c-jun* and other factors also regulate survivin expression. The survivin gene is regulated by a variety of factors including chronic hypoxia, growth factors, HIF1α (hypoxia-inducible factor), and paracrine factors. The independent role of these factors in ROS signaling to the survivin gene remains to be determined.

ACKNOWLEDGMENTS

This work was supported in part by National Institutes of Health (NIH) Grants R01CA70896, R01CA75503, and R01CA86072 (R.G.P.). The Kimmel Cancer Center is supported by the NIH Cancer Center Core Grant P30CA56036 (R.G.P.). This project is funded in part from the Dr. Ralph and Marian C. Falk Medical Research Trust and a grant from Pennsylvania Department of Health (R.G.P.), which specifically disclaims responsibility for analyses, interpretations, or conclusions.

REFERENCES

Albanese, C., *et al.* (1999). Activation of the *cyclin D1* gene by the E1A-associated protein p300 through AP-1 inhibits cellular apoptosis. J. Biol. Chem. *274*, 34186–34195.

Atabai, K., *et al.* (2005). Mfge8 is critical for mammary gland remodeling during involution. Mol. Biol. Cell *16*, 5528–5537.

Balaban, R. S., Nemoto, S., and Finkel, T. (2005). Mitochondria, oxidants, and aging. Cell *120*, 483–495.

Beauchamp, C., and Fridovich, I. (1971). Superoxide dismutase: improved assays and an assay applicable to acrylamide gels. Anal. Biochem. *44*, 276–287.

Behrens, A., Sibilia, M., and Wagner, E. F. (1999). Amino-terminal phosphorylation of c-Jun regulates stress-induced apoptosis and cellular proliferation. Nat. Genet. *21*, 326–329.

Bouras, T., Fu, M., Sauve, A. A., Wang, F., Quong, A. A., Perkins, N. D., Hay, R. T., Gu, W., and Pestell, R. G. (2005). SIRT1 deacetylation and repression of P300 involves lysine residues 1020/1024 within the cell-cycle regulatory domain 1. J. Biol. Chem. *280*, 10264–10276.

Boveris, A., and Chance, B. (1973). The mitochondrial generation of hydrogen peroxide. General properties and effect of hyperbaric oxygen. Biochem. J. *134*, 707–716.

Chang, L., Kamata, H., Solinas, G., Luo, J. L., Maeda, S., Venuprasad, K., Liu, Y. C., and Karin, M. (2006). The E3 ubiquitin ligase itch couples JNK activation to TNFalpha-induced cell death by inducing c-FLIP(L) turnover. Cell *124*, 601–613.

Church, S. L., Grant, J. W., Meese, E. U., and Trent, J. M. (1992). Sublocalization of the gene encoding manganese superoxide dismutase (MnSOD/SOD2) to 6q25 by fluorescence in situ hybridization and somatic cell hybrid mapping. Genomics *14*, 823–825.

Dohi, T., Beltrami, E., Wall, N. R., Plescia, J., and Altieri, D. C. (2004). Mitochondrial survivin inhibits apoptosis and promotes tumorigenesis. J. Clin. Invest. *114*, 1117–1127.

Dolado, I., Swat, A., Ajenjo, N., De Vita, G., Cuadrado, A., and Nebreda, A. R. (2007). p38alpha MAP kinase as a sensor of reactive oxygen species in tumorigenesis. Cancer Cell *11*, 191–205.

Edelman, E., Porrello, A., Guinney, J., Balakumaran, B., Bild, A., Febbo, P. G., Mukherjee, S. (2006). Analysis of sample set enrichment scores: assaying the enrichment of sets of genes for individual samples in genome-wide expression profiles. Bioinformatics *22*, e108–e116.

Eferl, R., Ricci, R., Kenner, L., Zenz, R., David, J. P., Rath, M., and Wagner, E. F. (2003). Liver tumor development. c-Jun antagonizes the proapoptotic activity of p53. Cell *112*, 181–192.

Fernandez-Pol, J. A., Hamilton, P. D., and Klos, D. J. (1982). Correlation between the loss of the transformed phenotype and an increase in superoxide dismutase activity in a revertant subclone of sarcoma virus-infected mammalian cells. Cancer Res. *42*, 609–617.

Ham, J., Babij, C., Whitfield, J., Pfarr, C. M., Lallemand, D., Yaniv, M., and Rubin, L. L. (1995). A c-Jun dominant negative mutant protects sympathetic neurons against programmed cell death. Neuron *14*, 927–939.

Hayakawa, M., Miyashita, H., Sakamoto, I., Kitagawa, M., Tanaka, H., Yasuda, H., Karin, M., and Kikugawa, K. (2003). Evidence that reactive oxygen species do not mediate NF-kappaB activation. EMBO J. *22*, 3356–3366.

Hettinger, K., Vikhanskaya, F., Poh, M. K., Lee, M. K., de Belle, I., Zhang, J. T., Reddy, S. A., and Sabapathy, K. (2007). c-Jun promotes cellular survival by suppression of PTEN. Cell Death Differ. *14*, 218–229.

Kamata, H., and Hirata, H. (1999). Redox regulation of cellular signalling. Cell Signal *11*, 1–14.

Kamata, H., Honda, S., Maeda, S., Chang, L., Hirata, H., and Karin, M. (2005). Reactive oxygen species promote TNFalpha-induced death and sustained JNK activation by inhibiting MAP kinase phosphatases. Cell *120*, 649–661.

Katiyar, S., Jiao, X., Wagner, E., Lisanti, M. P., and Pestell, R. G. (2007). Somatic excision demonstrates c-Jun induces cellular migration and invasion through induction of stem cell factor. Mol. Cell Biol. *27*, 1356–1369.

Kuan, C. Y., Yang, D. D., Samanta Roy, D. R., Davis, R. J., Rakic, P., and Flavell, R. A. (1999). The Jnk1 and Jnk2 protein kinases are required for regional specific apoptosis during early brain development. Neuron *22*, 667–676.

Kyriakis, J. M. (1999). Signaling by the germinal center kinase family of protein kinases. J. Biol. Chem. *274*, 5259–5262.

Lambeth, J. D. (2004). NOX enzymes and the biology of reactive oxygen. Nat. Rev. Immunol. *4*, 181–189.

Li, Z., Wang, C., Jiao, X., Katiyar, S., Casimiro, M. C., Prendergast, G. C., Powell, M. J., and Pestell, R. G. (2008). Alternate cyclin D1 mRNA splicing modulates p27KIP1 binding and cell migration. J. Biol. Chem. *283*, 7007–7015.

MacLaren, A., Black, E. J., Clark, W., and Gillespie, D. A. (2004). c-Jun-deficient cells undergo premature senescence as a result of spontaneous DNA damage accumulation. Mol. Cell. Biol. *24*, 9006–9018.

Melov, S. (2000). Mitochondrial oxidative stress. Physiologic consequences and potential for a role in aging. Ann. NY Acad. Sci. *908*, 219–225.

Mishin, V., Gray, J. P., Heck, D. E., Laskin, D. L., and Laskin, J. D. (2010). Application of the Amplex red/horseradish peroxidase assay to measure hydrogen peroxide generation by recombinant microsomal enzymes. Free Radic. Biol. Med. *48*, 1485–1491.

Neumeister, P., *et al.* (2003). Cyclin D1 governs adhesion and motility of macrophages. Mol. Biol. Cell *14*, 2005–2015.

Nohl, H., and Jordan, W. (1980). The metabolic fate of mitochondrial hydrogen peroxide. Eur. J. Biochem. *111*, 203–210.

Okado-Matsumoto, A., and Fridovich, I. (2001). Subcellular distribution of superoxide dismutases (SOD) in rat liver: Cu,Zn-SOD in mitochondria. J. Biol. Chem. *276*, 38388–38393.

Podar, K., *et al.* (2007). Up-regulation of c-Jun inhibits proliferation and induces apoptosis via caspase-triggered c-Abl cleavage in human multiple myeloma. Cancer Res. *67*, 1680–1688.

Radi, R., Turrens, J. F., Chang, L. Y., Bush, K. M., Crapo, J. D., and Freeman, B. A. (1991). Detection of catalase in rat heart mitochondria. J. Biol. Chem. *266*, 22028–22034.

Sage, J., Miller, A. L., Perez-Mancera, P. A., Wysocki, J. M., and Jacks, T. (2003). Acute mutation of retinoblastoma gene function is sufficient for cell cycle re-entry. Nature *424*, 223–228.

Sattler, M., Winkler, T., Verma, S., Byrne, C. H., Shrikhande, G., Salgia, R., and Griffin, J. D. (1999). Hematopoietic growth factors signal through the formation of reactive oxygen species. Blood *93*, 2928–2935.

Scherz-Shouval, R., Shvets, E., Fass, E., Shorer, H., Gil, L., and Elazar, Z. (2007). Reactive oxygen species are essential for autophagy and specifically regulate the activity of Atg4. EMBO J. *26*, 1749–1760.

Seaman, R. L. (1976). Comments on "propagation of plane waves through two parallel dielectric sheets." IEEE Trans. Biomed. Eng. *23*, 269–270.

Shaulian, E., and Karin, M. (2002). AP-1 as a regulator of cell life and death. Nat. Cell Biol. *4*, E131–E136.

Sinha, A. K. (1972). Colorimetric assay of catalase. Anal. Biochem. *47*, 389–394.

Tanaka, H., Matsumura, I., Ezoe, S., Satoh, Y., Sakamaki, T., Albanese, C., Machii, T., Pestell, R. G., and Kanakura, Y. (2002). E2F1 and c-Myc potentiate apoptosis through inhibition of NF-kappaB activity that facilitates MnSOD-mediated ROS elimination. Mol. Cell *9*, 1017–1029.

Temkin, V., and Karin, M. (2007). From death receptor to reactive oxygen species and c-Jun N-terminal protein kinase: the receptor-interacting protein 1 odyssey. Immunol. Rev. *220*, 8–21.

Udou, T., Hachisuga, T., Tsujioka, H., and Kawarabayashi, T. (2004). The role of c-jun protein in proliferation and apoptosis of the endometrium throughout the menstrual cycle. Gynecol. Obstet. Invest. *57*, 121–126.

Vleugel, M. M., Greijer, A. E., Bos, R., van der Wall, E., and van Diest, P. J. (2006). c-Jun activation is associated with proliferation and angiogenesis in invasive breast cancer. Hum. Pathol. *37*, 668–674.

Wang, C., *et al.* (2003). Cyclin D1 repression of peroxisome proliferator-activated receptor gamma (PPARgamma) expression and transactivation. Mol. Cell. Biol. *23*, 6159–6173.

Wang, P., Anton, M., Graham, F. L., and Bacchetti, S. (1995). High frequency recombination between loxP sites in human chromosomes mediated by an adenovirus vector expressing Cre recombinase. Somat. Cell Mol. Genet. *21*, 429–441.

Xia, Y., and Karin, M. (2004). The control of cell motility and epithelial morphogenesis by Jun kinases. Trends Cell Biol. *14*, 94–101.

Xia, Z., Dickens, M., Raingeaud, J., Davis, R. J., and Greenberg, M. E. (1995). Opposing effects of ERK and JNK-p38 MAP kinases on apoptosis. Science *270*, 1326–1331.

Zenz, R., Scheuch, H., Martin, P., Frank, C., Eferl, R., Kenner, L., Sibilia, M., and Wagner, E. F. (2003). c-Jun regulates eyelid closure and skin tumor development through EGFR signaling. Dev. Cell *4*, 879–889.

Zhou, X., Gallazzini, M., Burg, M. B., and Ferraris, J. D. (2010). Contribution of SHP-1 protein tyrosine phosphatase to osmotic regulation of the transcription factor TonEBP/OREBP. Proc. Natl. Acad. Sci. USA *107*, 7072–7077.